Materials Research Proceedings 44 (2024) 482-492 https://doi.org/10.21741/9781644903254-52

Modelling of dynamic scale layer growth considering temperature, time and alloying elements

BERGELT Tim[1,a] *, GRAF Marcel[1,b], HUNZE-TRETOW Jan[2,c], BEHRENS Bernd-Arno[2,d] and LAMPKE Thomas[1,e]

[1]Materials and Surface Engineering Group, Institute of Materials Science and Engineering, Chemnitz University of Technology, 09107 Chemnitz, Germany

[2]Institute for Forming Technology and Forming Machines, Leibniz University Hannover, 30823 Garbsen, Germany

[a]tim.bergelt@mb.tu-chemnitz.de; [b]marcel.graf@mb.tu-chemnitz.de, [c]hunze@ifum.uni-hannover.de, [d]behrens@ifum.uni-hannover.de, [e]thomas.lampke@mb.tu-chemnitz.de

Keywords: Scale Layer, Microstructure, Thermophysical Properties, Modelling

Abstract: During hot forming of steel oxide scaling occurs at higher temperatures caused by reactions with oxide containing atmospheres. Three characteristic iron oxides exist for steel at temperatures above 570°C: Wustite (FeO), magnetite (Fe_3O_4) and hematite (Fe_2O_3). Scale layer formation is influenced by various process parameters, such as temperature, process time and furnace atmosphere. Additionally, the base material with different alloying elements (e.g. C, Cr, Si and Ni) also affects the scale layer formation. Therefor oxide scales are very difficult to handle in the entire manufacturing process. The aim of this work is to examine and evaluate the influence of temperature, time and the alloying elements C and Cr in association with the layer growth, layer composition and thermophysical properties for scale layers. Based on the achieved correlations, a model is developed, which is able to predict the scale formation and scale properties, depending on temperature, time and alloying elements. With rising temperature and time increasing layer thicknesses were observed. Further, the additional Cr ensured lower layer thicknesses compared to the unalloyed steels. The iron oxide distribution changed with rising temperature to higher oxide containing phases like magnetite and hematite. The mathematical model, developed based on this results, is able to calculate the resulting layer structure, thickness and thermophysical properties depending on temperature, time and chemical composition of the material.

Introduction

During the hot forming of metals, such as forging or rolling, the material surface reacts with oxide-containing atmospheres at temperatures above 570°C. Consequently, a new solid phase is formed at the material's surface: the oxide scale. These scale layers usually consist of three iron oxides: Wustite FeO, magnetite Fe_3O_4 and hematite Fe_2O_3. The scale layer formed during hot forming processes causes material loss and damages the forming tools and workpieces. Hence, a better understanding of scale layer growth and scale layer properties could reduce material losses and damage, enabling more cost and resource efficient production processes.

It is well known from the literature that scale layer formation depends on different process parameters, such as temperature, time and alloying composition of the base material [1,2]. *Graf et al.* [3] determined the influence of time and temperature on the scale development. The scale layer thickness increases with higher temperatures and longer process times due to the enhanced diffusion processes with rising temperatures. Furthermore, an increase in carbon content leads to a decrease in scale layer thickness. Besides carbon, other alloying elements, notably chromium, influence the scale layer formation. In case of Cr steels, the microstructure comprises additional

chromium precipitates (chromium spinels and chromium(III) oxide), which inhibit the surface oxidation processes, thereby leading to a decreased scale layer formation [4,5].

Therefore, detailed knowledge of the thermophysical properties of the scale layer is required as they differ from the base material to optimize the hot forming processes. The scale layer may act as a barrier for the workpiece and influence the thermal behaviour of the entire system due to the different thermophysical properties [2]. To model a thermomechanical process, the material's mechanical properties and stress collective, as well as the thermal properties of the modelling materials, need to be known. For thermo-mechanical process modelling, the important properties are thermal conductivity λ, thermal expansion coefficient α and specific heat capacity c_p. Since the fractions of iron oxides within the scale layer can vary based on the process conditions, it is necessary to determine the thermophysical properties of each iron oxide to predict the thermophysical properties of the complete scale layer. *Dubey et al.* [6] developed a numerical heat conduction model to predict the transient three-dimensional temperature field in billets, considering the scale layer growth on the billet surfaces during the reheating simulations. However, the scale layer was only described using the iron oxide wustite without considering the other two oxide types. In addition, the layer growth was only modelled using the parabolic law, as the study focused on longer application times of the temperature. The resulting models can predict process influences on the temperature field and the scale growth of the billets. Especially for scale growth, different growth rates can be determined depending on the temperature of the furnace gas. The maximum scale layer thicknesses were identified at the locations with the highest temperature on the billet. The hot rolling model developed by *Krzyzanowski et al.* [7] describes the influences of the scale layer composition, crack formation and propagation during the rolling process and the material flow of the formed material. To simplify the model, *Krzyzanowski et al.* chose a 2D model. The scale layer consists of individual oxide fragments connected to each other. The size of the individual fragments is based on the experimentally determined crack distances, and it is less than the smallest detected crack distance, allowing a prediction of the crack distances and predictions about the crack distribution over the entire scale layer. However, this model does not simulate the scale layer growth during the heating process; instead, it employs a predefined scale layer as an initial step. As a result, the model cannot simulate various process conditions during the heating.

Materials and experimental

Material. In this work, the influence of carbon and chromium on the scale formation is investigated by a separate and comparative analysis of the element's influences. Therefore, seven different steels were used. The chemical composition of the steels, determined by melt analysis, is listed in Table 1.

Table 1. Chemical composition of the seven analysed steels.

Steel	C	Si	Mn	P	S	Cr	Mo	Ni	Cu	Al
C15	0.16	0.21	0.42	<0.001	<0.001	0.1	0.045	0.087	0.108	0.017
15Cr3	0.16	0.21	0.42	<0.001	<0.001	0.6	0.045	0.087	0.108	0.017
C45	0.49	0.2	0.42	<0.004	<0.001	0.1	0.034	0.081	0.096	0.021
45Cr3	0.49	0.2	0.42	<0.004	<0.001	0.6	0.034	0.081	0.096	0.021
45Cr4	0.49	0.2	0.42	<0.004	<0.001	1.15	0.035	0.076	0.1	0.017
C60	0.63	0.2	0.42	<0.001	<0.001	0.1	0.035	0.076	0.1	0.017
60Cr3	0.63	0.2	0.42	<0.001	<0.001	0.6	0.035	0.076	0.1	0.017

Three different C steels (C15, C45 and C60) were chosen to analyse the influence of carbon. Further, four different Cr steels (15Cr3, 45Cr3, 45Cr4 and 60Cr3) were selected to determine the influence of chromium. Using C45, 45Cr3 and 45Cr4 three different chromium contents are available for the same carbon concentration of 0.49 wt. %. The influence of the chromium content will be focussed predominantly on this steel series.

Scale formation and analysis. To determine the influence of temperature and time on the scale layer growth, each steel was subjected to scaling at temperatures of 900, 1050 and 1200°C for 20, 40 and 120 s durations, respectively. These scaling tests were performed on a quenching dilatometer (DIL805 A/D, Bähr) with cylindrical samples of 10 mm in height and 10 mm in diameter. The samples were inductively heated, and the temperature was monitored and controlled by using thermocouples. The closed test chamber of the dilatometer allowed a defined atmosphere containing argon during heating and cooling to prevent pre- and post-scaling. During the scaling process, the test chamber was flooded with atmosphere. The heating and cooling rates, and the gas flow, were set identically over the entire series of tests. After scaling, the samples were embedded in epoxy resin to protect the scale layer from further damage. Besides, cross sections were metallographically prepared for all scaled samples to identify the scale layer thickness and the iron oxide distribution depending on the temperature and time regime. The cross-sections were then analysed using light microscopy (OLYMPUS GX51 inverted optical microscope).

Dilatometer, DSC and LFA analysis. In addition to the scale layer growth and scale layer structure, the thermophysical properties of thermal expansion, specific heat capacity and thermal conductivity were determined for a complete scale layer. To account for the influence of the base materials and the layer growth, the base material was scaled to generate the pure scale samples. This contrasts with most other studies, in which classic iron oxide powder represents the scale layer. To produce pure scale samples, the scale layer requires a thickness of 3–4 mm. Therefore, cylindrical samples were scaled in the furnace at 900, 1050 and 1200°C up to 96 hours. For 900°C a thickness of 2 mm could not be achieved and for 1200 °C the scale layer showed intense cracking and high porosity compared to the scale layers produced at 1050°C. For further analyses, the material was scaled at 1050°C for 96 h. The 3–4 mm thick scale layer was separated from the substrate using a cutting machine and reduced to the required dimensions by manual grinding. The investigation of the thermophysical properties was focused on C45, 45Cr3 and 45Cr4 to reduce the number of necessary tests.

Further, thermal expansion was determined by using a dilatometer (*DIL402E, NETZSCH GmbH & Co. Holding KG*). The pure scale sample was measured from RT (room temperature) up to 1200 °C at a heating rate of 5 K/min and adjusted with the reference measurement. The specific heat capacity was determined using Differential scanning calorimetry (DSC) on *STA449J* (*NETZSCH GmbH & Co. Holding KG*). For the experiments, pure scale samples were pulverised and tested between RT and 1200 °C with a heating and cooling rate of 5 K/min. Based on preliminary investigations, it was impossible to determine the thermal conductivity of the pure scale samples using laser flash analysis. Due to the porous and heterogeneous layer structure of the entire scale layer, no comparative results could be obtained. Therefore, the modelling steps will use comparative literature data [8–13].

Modelling

To utilise the obtained data for a prediction model, all results and their dependencies need to be described by mathematical equations. To reduce the complexity of all experimental data, the layer growth, layer composition and thermophysical properties are considered separately and combined using a *Fortran-77* script. By choosing *Fortran-77* as the programming language, the integration to the Solver: *MSC.Marc* within *Simufact Forming* can be used in future works to implement the scale layer model in the simulations of hot forming processes. To describe the experimental data obtained in Scale formation and analysis and Dilatometer, DSC and LFA analysis for scale layer growth, scale layer structure and thermophysical properties as a function of temperature and time it is necessary to describe and fit the data via mathematical equations. For the iron oxide distribution of the scale layer, a classic polynomial fit is used, allowing a sufficiently high coefficient of determination for the experimental data. Due to the characteristics of the

experimental data, a separate fit is necessary for temperatures up to 1050°C and above 1050°C, as the curve characteristics change significantly at this point and a fit over the entire temperature range provides poor results. To describe the iron oxide evolution up to 1050°C for wustite and magnetite as well as for hematite, a polynomial of 7th degree (Eq. 1) is used. For temperatures above 1050°C, a polynomial of 3rd degree (Eq. 2) is accurate enough. In the polynomial equations, B0–B7 are coefficients and y is the volume fraction of the respective iron oxide from 100 % volume fraction.

$$y = B0 + B1 \cdot x^1 + B2 \cdot x^2 + B3 \cdot x^3 + B4 \cdot x^4 + B5 \cdot x^5 + B6 \cdot x^6 + B7 \cdot x^7 \quad (1)$$

$$y = B0 + B1 \cdot x^1 + B2 \cdot x^2 + B3 \cdot x^3 \quad (2)$$

For scale layer growth, the ARRHENIUS approach (Eq. 3) is used as a combined linear and parabolic layer growth model to describe the resulting layer thickness as a function of temperature and time for all steels.

$$d_{oxid} = -\frac{k_{p0}*\exp\left(\frac{-Q_p}{R*T}\right)}{2*k_{l0}*\exp\left(\frac{-Q_l}{R*T}\right)} + \sqrt{\left(\frac{k_{p0}*\exp\left(\frac{-Q_p}{R*T}\right)}{2*k_{l0}*\exp\left(\frac{-Q_l}{R*T}\right)}\right)^2 + k_{p0} * \exp\left(\frac{-Q_p}{R*T}\right) * t_{oxidation}} \quad (3)$$

Where d_{oxid} is the scale layer thickness, R is the universal gas constant and T is the scaling temperature. The model coefficients are k_{p0}, k_{l0}, Q_p and Q_l. The coefficients were determined using the least squares method for all process parameter variations to achieve a high coefficient of determination. For the thermophysical properties (thermal expansion, specific heat capacity and thermal conductivity), it is only possible to measure experimentally fixed scale layer compositions (see Thermophysical properties). Further, to obtain a dynamic model, it is necessary to know the thermophysical properties of each iron oxide as a function of temperature. Only then it is possible to predict the thermophysical properties for each scale layer composition by using a weighting function combined with the iron oxide distribution model. The required data for the individual iron oxides is taken from the literature [8–13] and validated experimentally using the pure scale samples.

Results and Discussion

Iron oxide distribution. To characterise the scale layers, light microscopy images were taken of all scaled samples. The microscopic scale layers at 1200°C for 120 s for C15 and 15Cr3 are shown in Fig. 1. In both images, the three-layer system is noticeable, which allows the identification of the different iron oxide types through various grey colours [14]. The dark grey area on the bottom of the scale layer is wustite (FeO), the slightly brighter layer on top is magnetite (Fe_3O_4) and the brightest layer near to the surface is hematite (Fe_2O_3).

The resulting iron oxide distribution was determined based on the light microscopy images of all parameter constellations for the seven steels. The measured distribution is described as a proportion of 100 % with the entire layer. For C and Cr steels, similar tendencies could be achieved for 900, 1050 and 1200°C. At scaling temperatures at 900 and 1050°C, wustite dominates with over 80 % volume fraction. Magnetite occurs at less than 20 % and hematite is formed at a maximum of up to 1 % (see Fig. 2: B and C). For 1200 °C, the proportions of wustite and magnetite vary between 40–50 % and hematite exhibits a constant volume fraction of 10 % (see Fig. 2: D). Generally, an increase in temperature leads to a change in the iron oxide distribution inside the scale layer. With higher temperatures, more hematite forms at the expense of wustite and magnetite. Also, with temperatures over 1050°C, wustite and magnetite get more equally balanced up to 1200°C. However, it can be assumed that with a further temperature increase, wustite will

continue to decrease in favour of magnetite and hematite. The volume fraction of wustite, magnetite and hematite show no significant change with rising time. This distribution of the oxides is also described in literature [15].

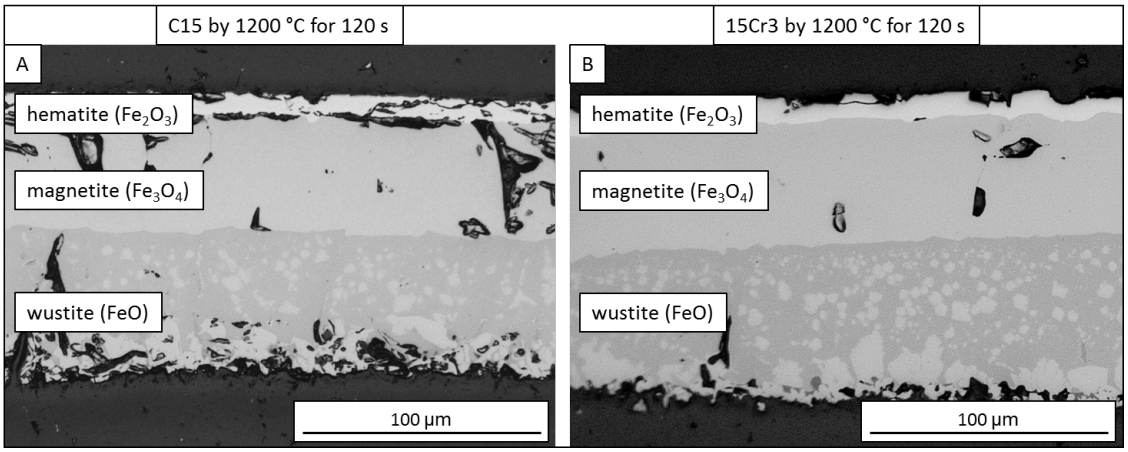

Fig. 1. Distribution of the three iron oxides (wustite, magnetite and hematite) within a scale layer produced at 1200 °C for 120 s for the material C15 (A) and 15Cr3 (B).

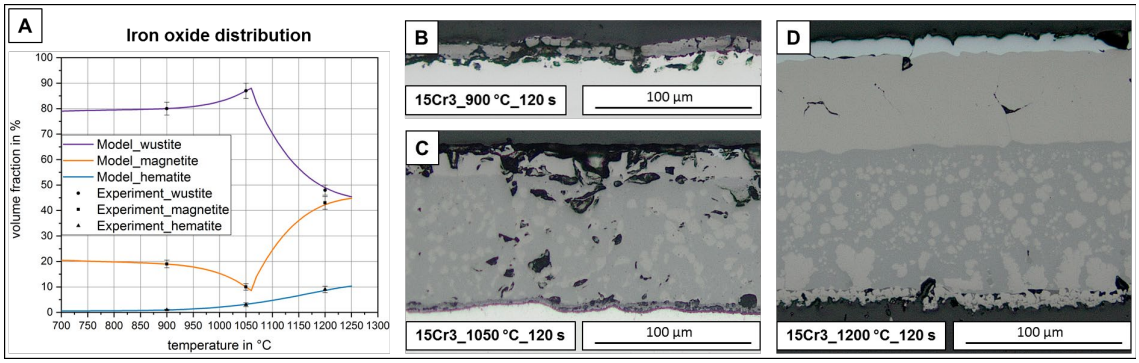

Fig. 2. A: Iron oxide distribution as a volume fraction in % over the scaling temperature for each iron oxide (wustite, magnetite and hematite). The colored curves display a polynomial fit based on the experimental data (black points). B: scale layer for 15Cr3 after 120 s at 900°C. C: scale layer for 15Cr3 after 120 s at 1050°C. D: scale layer for 15Cr3 after 120 s at 1200°C.

To describe the layer composition via mathematical equations, only the influence of various temperatures is considered. The time variation is too small and will be cut out for simplification. Furthermore, no differences were found in the iron oxide distribution in the resulting scale layer between the different steel alloys, so that one model can be used for all steel compositions. The mathematical approach, described in chapter Modelling, using a polynomial fit is shown in Fig. 2: A. The determined coefficients B0–B7 for the polynomial fits are listed in Table 2.

Table 2. Coefficients B0–B7 for each iron oxide for temperatures up to 1050°C and from 1050°C.

Phase		B0	B1	B2	B3	B4	B5	B6	B7
FeO	up to 1050 °C	73.992	0.0413	-3.32e-4	1.52e-6	-3,79e-9	5.26e-12	-3.8e-15	1.11e-18
	from 1050 °C	6030	-13.913	1.08e-2	-2.8e-6	-	-	-	-
Fe_3O_4	up to 1050 °C	26.094	-0.0437	3.58e-4	-1.65e-6	4.1e-9	-5.8e-13	4.22e-15	-1.2e-18
	from 1050 °C	-5135	12.019	-0.0093	2.4e-6	-	-	-	-
Fe_2O_3	from 900 °C	1.7651	-0.0388	3.14e-4	-1.24e-6	2.64e-9	-3.1e-12	1.81e-15	-4.2e-19

The proportion of wustite (purple curve) rises to a maximum of 1050°C and then decreases to approximately 45 % at 1200°C. The proportion of magnetite initially decreases until 1050°C and begins to increase from 1050°C. The scale layer contains almost no hematite at temperatures around 900°C. However, with temperatures above, the amount of hematite increases continuously with increasing temperature. The black points represent the experimental data, and the model curves are in very good agreement with this data. However, the model can only be considered as a first approximation, since there are not enough reference points. Therefore, only a coarse extrapolation between the reference points can be applied. In future works, the model shown in Fig. 2: A must be supported with further data and need to be updated.

Influence of temperature, time and material. Based on the light microscopy images shown in chapter Iron oxide distribution, the resulting layer thicknesses were evaluated as a function of the temperature and time. The below graphs (Fig. 3) illustrates the variation in layer thickness over time for 900, 1050 and 1200°C. The selected curves compare various C content (Fig. 3: A) and Cr content (B). The layer growth of each steel corresponds to the established √t–law for layer growth kinetics.

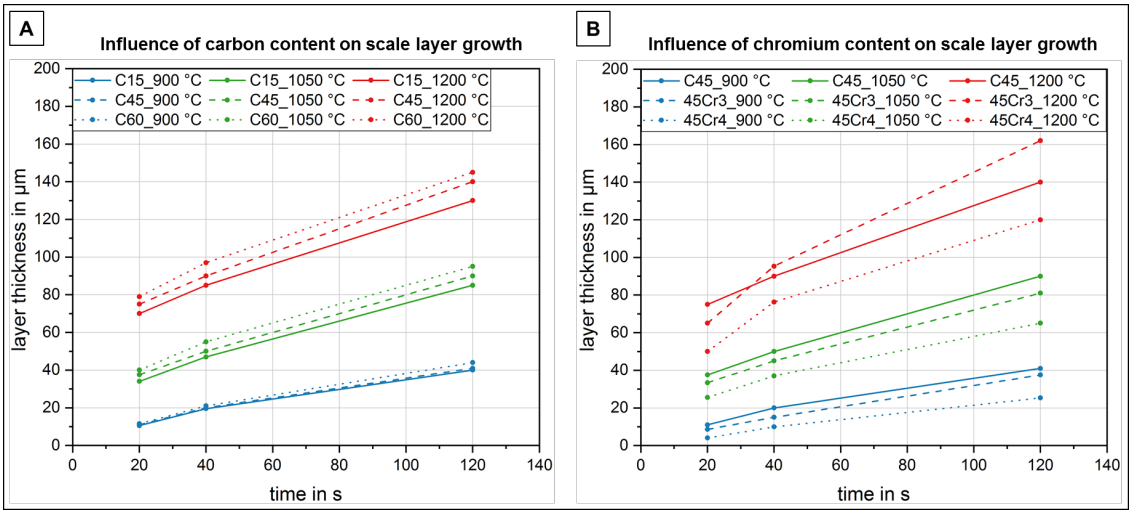

Fig. 3. Layer thickness of the resulting oxide layer over time for three temperatures 900, 1050 and 1200°C. A: comparison between C15, C45 and C60. B: comparison of two selected Cr-steels 45Cr3 and 45Cr4 and the chromium-free C45.

The oxide scale growth will slow down with increasing time, but never stop completely. Nevertheless, the interesting area is within the first few minutes, due to the point of highest oxide scale growth and can be extrapolated for longer periods according to the parabolic law. In addition to time, an increasing scaling temperature ensures thicker layers. As the temperature increases the activation energy increases, which is directly associated with enhanced diffusivity of the reactants. The layer growth is completely diffusion-controlled, so an increase in temperature results automatically in higher layer thicknesses. It is observed that as carbon content rises, layer thickness

Materials Research Proceedings 44 (2024) 482-492 https://doi.org/10.21741/9781644903254-52

increases (Fig. 3: A). This tendency corresponds to the development of the austenitic grain size over the carbon content. It was determined that the average grain size increases with higher carbon content. For the scale layer, it can be concluded that a higher number of grain boundaries in the microstructure lead to a thinner layer thickness. As an explanation, the grain boundaries act as slight diffusion barriers and seem to affect the layer growth. This effect can be observed for all three temperatures.

Further, the influence of the different Cr content on the layer thickness of C45, 45Cr3 and 45Cr4 (Fig. 3: B) shows an increase in layer thickness with rising temperature, comparable to the C steels. Moreover, it could be determined that the layer thickness decreases with increasing Cr content. Between 45Cr3 and 45Cr4, a significantly higher influence of the chromium content on the layer thickness is observed compared to C45 and 45Cr3. The chromium-free C45 shows the highest layer thicknesses, but only slightly above that for the 45Cr3. This effect is most likely the result of chromium precipitations, which act as slight diffusion barriers during layer formation and hinder the layer growth. With rising Cr content, this effect seems to increase. However, for 45Cr3 at 1200 °C, a pronounced increase in layer thickness was observed, which cannot be explained by literature currently.

To describe the correlations between temperature and time on the layer growth in a single equation, the ARRHENIUS-approach, described in Modelling, was used. The four unknown coefficients k_{p0}, k_{l0}, Q_p and Q_l were determined using a least square fit (see Table 3) and allow a description of the scale layer thickness based on the temperature and time as inputs. In the current state it was impossible to establish factorial relationships between the coefficients to describe the influence of the chemical composition in the base material. Therefore, the coefficients for each material must be defined separately in the scale layer model and the layer thickness can only be predicted accurately for the analysed steels.

Table 3. Coefficients k_{p0}, k_{l0}, Q_p and Q_l from the ARRHENIUS-approach for each steel to describe the scale layer growth dependent on temperature and time.

Steel	k_{p0} in µm²/s	Q_p in J/mol	k_{l0} in µm/s	Q_l in J/mol
C15	1.76e+06	1.14e+05	9.89e+06	1.47e+05
15Cr3	1.37e+07	1.35e+05	2.11e+07	1.69e+05
C45	2.15e+06	1.14e+05	2.11e+07	1.57e+05
45Cr3	2.14e+07	1.40e+05	2.10e+07	1.63e+05
45Cr4	4.03e+06	1.26e+05	2.12e+07	1.72e+05
C60	1.85e+06	1.11e+05	2.58e+07	1.59e+05
60Cr3	9.97e+06	1.29e+05	2.10e+07	1.65e+05

Fig. 4 shows the fits for C45 (A), 45Cr3 (B) and 45Cr4 (C) as examples for all seven steels. Identical to Fig. 3, the scale layer thickness is plotted over time. The coloured points indicate the experimentally measured layer thickness at the respective temperature and time. The solid lines represent the fit using the ARRHENIUS-approach for temperatures at 900, 1050 and 1200°C. For most of the curves, a coefficient of determination (R^2) with a value over 0.9 was achieved, with only a few curves falling between 0.8 and 0.9. Based on the obtained R^2 between the fit and the experiments, the coefficients (k_{p0}, k_{l0}, Q_p and Q_l) for each tested steel are validated.

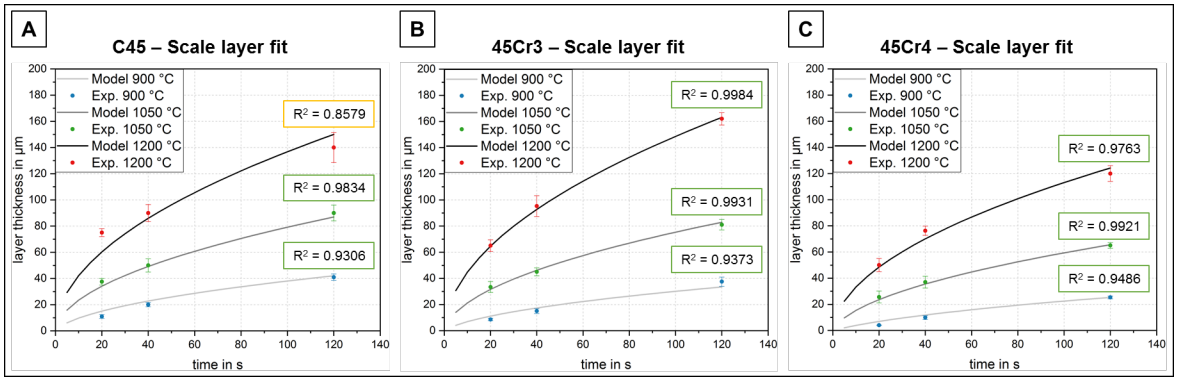

Fig. 4. Scale growth for C45 (A), 45Cr3 (B) and 45Cr4 (C) based on the calculated coefficients of the ARRHENIUS-approach (solid lines) for 900, 1050 and 1200 °C. Compared with the experimental data (colored points), a sufficiently high coefficient of determination was achieved for each curve.

Thermophysical properties. As stated in chapter Iron oxide distribution, the distribution of the iron oxides inside the scale layer changes as a function of temperature. Due to the distinct thermophysical properties of every iron oxide, the properties of the resulting scale layers also vary at different temperatures. It was impossible to produce samples consisting of only one iron oxide (wustite, magnetite or haematite), therefore pure scale samples of a complete layer system were used. These scale samples were produced at 1050°C in a furnace, resulting in an iron oxide distribution of 80 % wustite, 19 % magnetite and 1 % hematite. Nevertheless, in all three experiments to determine the thermophysical properties, an oxidation reaction was detected in the first heating cycle up to 1200 °C. In all further test cycles from RT up to 1200°C, no further oxidation peaks were observed. The oxidation in the first heating cycle caused a change in the iron oxide distribution to 0 % wustite, 30 % magnetite and 70 % hematite. The lack of bonding between the scales and the base material results in the consumption of the wustite phase and the high temperature phase haematite with remaining magnetite is formed. The assumption is that the 0-30-70 distribution is always achieved with pure scale samples, regardless of the scale layer structure before the first heating cycle. Based on this result, the determined experimental data will be validated using a model based on literature data for exactly this 0-30-70 distribution.

For the thermal expansion α, data was taken from the publication by *Beygelzimer* [16] for all three iron oxides and the α for the 0-30-70 distribution was calculated using a weighting function. The experimentally measured thermal expansion coefficients for the pure scale samples based on the steels C45 (green), 45Cr3 (yellow) and 45Cr4 (orange) is illustrated in Fig. 5: A. In addition, the black curve shows the expansion model of the 0-30-70 distribution based on the literature data. The experimental curves of the three scale samples are slightly below the model curve and show a peak at approximately 630 °C where the model detects it around 590°C. These slight differences can be explained by the additional alloying elements such as chromium and silicon, which are also present in the pure scale samples based on the base material. However, this assumption cannot be confirmed currently by experimental data. The slightly higher curve of 45Cr4 compared to C45 and 45Cr3 is also attributed to the influence of the additional chromium in the scale samples. Nevertheless, it can be concluded that the thermal expansion model can represent real conditions with sufficient accuracy, so it can be used further in the scale layer model.

For the specific heat capacity c_p, the same procedure was chosen as for the thermal expansion. The experimental data were determined using pure scale samples for DSC testing and the heat capacity model was developed, based on the literature data of the individual iron oxides according to *Beygelzimer* [17].The experimental data of the pure scale samples based on C45 (green), 45Cr3 (yellow) and 45Cr4 (orange) with the model curve (black) for the 0-30-70 distribution is shown in Fig. 5: B. For the specific heat capacity, the model curve shows a very good correlation with the

experimental data for the 45Cr3 and 45Cr4. The C45 appears to be clearly higher, compared to the model curve. These differences can be explained by the additional alloying elements such as chromium and silicon, which are also present in the pure scale samples based on the base material. However, currently it is unexplainable why the samples with higher chromium closer to the model curve. Therefore, further investigations are needed. Both peaks at 575°C and 690°C matches exactly for each material. Only at temperatures above 1000°C, the experimental curve increases significantly more compared to the literature data. In the temperature range from RT to 1000°C, the heat capacity model is validated based on the experimental data. In accordance with [18,19], the literature data will be used from a temperature of 1000°C and above.

To determine the thermal conductivity λ, pure scale samples were analysed using LFA (Laser Flash Analysis). Due to the partially high porosity and strong heterogeneity of the scale layer, it was impractical to generate reproducible and valid results. Therefore, the thermal conductivity will be determined solely based on the literature data. The thermal conductivity model is developed according to the data from *Beygelzimer* [13] for each iron oxide and was validated using further literature [8–12]. The thermal conductivity for three exemplary layer compositions are displayed in Fig. 5: C. The 70-30-0 distribution represents a scale layer at 900°C and the 45-45-10 distribution represents a scale layer at 1200°C. The 0-30-70 distribution represents the known distribution after further oxidation without bonding to the substrate material. The three model curves demonstrate clearly that scale formed at different heating temperatures has different thermophysical properties and this fact has to be taken into account in the modelling of scale layers.

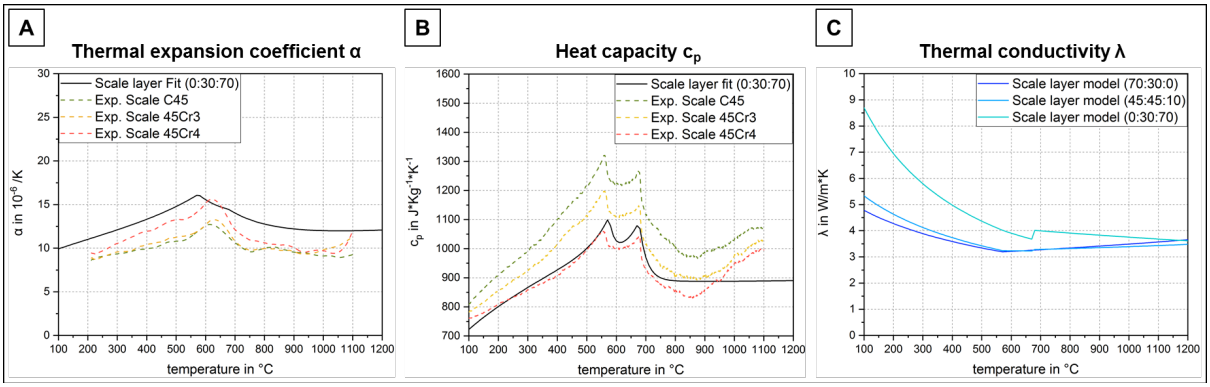

Fig. 5: A: Calculated thermal expansion coefficient using the weighting function based on the literature data of Beygelzimer [16] for a 0-30-70 distribution. Compared with the experimental data (colored lines), the model shows good agreement. B: Calculated heat capacity using the weighting function based on the literature data of Beygelzimer [17] for a 0-30-70 distribution. Up to a temperature of 850°C, model and experimental curves show very good agreement. After that, the experimental curves differ greatly from the literature. C: Calculated thermal conductivity using the weighting function based on the literature data of Beygelzimer [13] for a 70-30-0, 45-45-10 and 0-30-70 distribution.

All the equations and coefficients determined for the iron oxide distribution, the scale layer growth and the thermophysical properties were finally implemented in a *Fortran-77* script to predict the expected scale layer thickness, layer composition and the resulting properties by entering the temperature and time. As all sub-models (iron oxide distribution, scale layer growth and thermophysical properties) were considered to be validated, this also applies for the complete scale layer model. In future work, this model will be used in hot forming simulations with the FE program *Simufact Forming*. This enables the detection of the influence of different scale layers on heating and forming, as well as optimisation to reduce or systematically adjust scale layers.

Conclusions

The aim of this work was to create a scale layer model that can predict the resulting scale layer thickness and structure with associated thermophysical properties as a function of temperature, time and chemical composition. To accomplish this goal, seven different steels with varying carbon and chromium contents were scaled.

- Higher carbon content increases layer thickness, while additional chromium content leads to smaller layer thicknesses.
- High agreement between ARRHENIUS-fit and experimental data, allowed the use of the layer growth model outside the reference points.
- Carbon and chromium have a relatively small influence on the iron oxide composition of the scale layer. With higher temperatures significantly more hematite is formed and wustite and magnetite are evenly distributed.
- The thermophysical properties of the scale layer focussed on thermal expansion α, and specific heat capacity c_p could be determined using pure scale samples
- The models for thermal expansion, heat capacity and thermal conductivity were created using data from the literature and experimentally validated.
- In *Fortran-77* a Scale-Model was developed that can predict the scale layer thickness, iron oxide distribution and thermophysical properties for any temperature and time.

In future works, the scale layer model will be used in hot forming simulations with the FE programme *Simufact Forming* to consider scale formation during heating and forming processes. Another field of application could be the optimisation of furnace strategies with the aim of reducing scale formation or for the systematic adjustment of required scale layer properties.

Funding

The authors would like to thank the German Research Foundation (DFG) for funding the research project “Generally modelling of material behavior and surface modifications for FEM analysis of die forging of carbon steels” (grant number 316273316).

Author Credits

The author would like to thank Stephan Daniel Schwöbel from TU Chemnitz/Germany for the support in developing the fits, Max Müller from TU Chemnitz/Germany for the work at the dilatometer and metallographic preparation.

References

[1] R.M. Pineda Huitron, P.E. Ramírez López, E. Vuorinen, P. Nazen Jalali, L. Pelcastre, M. Kärkkäinen, Scale Formation on HSLA Steel during Continuous Casting Part I: The Effect of Temperature–Time on Oxidation Kinetics, Metals 10 (2020) 1243. https://doi.org/10.3390/met10091243

[2] E. Wielgosz, T. Kargul, J. Falkus, Comparison of experimental and numerically calculated thermal properties of steels, METAL 2014 - 23rd International Conference on Metallurgy and Materials, Conference Proceedings (2014).

[3] M. Graf, M. Ullmann, G. Korpala, H. Wester, B. Awiszus, R. Kawalla, B.-A. Behrens, Forming and Oxidation Behavior During Forging with Consideration of Carbon Content of Steel, Metals 8 (2018) 996. https://doi.org/10.3390/met8120996

[4] D.J. Young, J. Zurek, L. Singheiser, W.J. Quadakkers, Temperature dependence of oxide scale formation on high-Cr ferritic steels in Ar–H2–H2O, Corrosion Science 53 (2011) 2131–2141. https://doi.org/10.1016/j.corsci.2011.02.031

[5] F.H. Stott, G.C. Wood, J. Stringer, The influence of alloying elements on the development and maintenance of protective scales, Oxid Met 44 (1995) 113–145. https://doi.org/10.1007/BF01046725

[6] S.K. Dubey, P. Srinivasan, Development of three dimensional transient numerical heat conduction model with growth of oxide scale for steel billet reheat simulation, International J. Therm. Sci. 84 (2014) 214–227. https://doi.org/10.1016/j.ijthermalsci.2014.05.022

[7] M. Krzyzanowski, J.H. Beynon, Modelling the Behaviour of Oxide Scale in Hot Rolling, ISIJ Int. 46 (2006) 1533–1547. https://doi.org/10.2355/isijinternational.46.1533

[8] M. Takeda, T. Onishi, S. Nakakubo, S. Fujimoto, Physical Properties of Iron-Oxide Scales on Si-Containing Steels at High Temperature, Mater. Trans. 50 (2009) 2242–2246. https://doi.org/10.2320/matertrans.M2009097

[9] T. Akiyama, H. Ohta, R. Takahashi, Y. Waseda, J. Yagi, Measurement and Modeling of Thermal Conductivity for Dense Iron Oxide and Porous Iron Ore Aggliomerates in Stepwise Reduction, ISIJ Int. 32 (1992) 829–837. https://doi.org/10.2355/ISIJINTERNATIONAL.32.829

[10] J. Slowik, G. Borchardt, C. Köhler, R. Jeschar, R. Scholz, Influence of oxide scales on heat transfer in secondary cooling zones in the continuous casting process, part 2: determination of material properties of oxide scales on steel under spray-water cooling conditions, Steel Res. 61 (1990) 302–311. https://doi.org/10.1002/srin.199000353

[11] J. Mo/lgaard, W.W. Smeltzer, Thermal Conductivity of Magnetite and Hematite, J. Appl. Phys. 42 (1971) 3644–3647. https://doi.org/10.1063/1.1660785

[12] Y. Grosu, A. Faik, I. Ortega-Fernández, B. D'Aguanno, Natural Magnetite for thermal energy storage: Excellent thermophysical properties, reversible latent heat transition and controlled thermal conductivity, Solar Energy Materials and Solar Cells 161 (2017) 170–176. https://doi.org/10.1016/j.solmat.2016.12.006

[13] E. Beygelzimer, Y. Beygelzimer, Thermal conductivity of oxide scale and its components in the range from 0 C to 1300 C: Generalized estimates with account for movability of phase transitions, 2021.

[14] R.Y. Chen, W.Y.D. Yuen, A Study of the Scale Structure of Hot-Rolled Steel Strip by Simulated Coiling and Cooling, Oxid. Met. 53 (2000) 539–560. https://doi.org/10.1023/A:1004637127231

[15] G. Korpała, M. Ullmann, M. Graf, H. Wester, A. Bouguecha, B. Awiszus, B.-A. Behrens, R. Kawalla, Modelling the influence of carbon content on material behavior during forging, Penang, Malaysia, Author(s), 2017, p. 190013

[16] E. Beygelzimer, Y. Beygelzimer, Generalized estimates for thermal expansion of oxide scale in the range from 0C to 1300C with account for movability of phase transitions in its components, 2021.

[17] E. Beygelzimer, Y. Beygelzimer, Heat Capacity of oxide scale in the range from 0 C to 1300 C: Generalized estimates with account for movability of phase transitions, 2021.

[18] F. Grønvold, A. Sveen, Heat capacity and thermodynamic properties of synthetic magnetite (Fe3O4) from 300 to 1050 K. Ferrimagnetic transition and zero-point entropy, J. Chemic. Thermodynamic. 6 (1974) 859–872. https://doi.org/10.1016/0021-9614(74)90230-4

[19] J.P. Coughlin, E.G. King, K.R. Bonnickson, High-temperature Heat Contents of Ferrous Oxide, Magnetite and Ferric Oxide 1, J. Am. Chem. Soc. 73 (1951) 3891–3893. https://doi.org/10.1021/ja01152a098